Position of Transmembrane Helix 6 Determines Receptor G Protein Coupling Specificity

Alexander S. Rose,[†,‡] Matthias Elgeti,[†,∇] Ulrich Zachariae,[§] Helmut Grubmüller,[∥] Klaus Peter Hofmann,[†,⊥] Patrick Scheerer,[†,#] and Peter W. Hildebrand*[,†,‡]

[†]Institut für Medizinische Physik und Biophysik, [‡]AG ProteiInformatics, and [#]AG Protein X-ray Crystallography, Charité—Universitätsmedizin Berlin, Charitéplatz 1, 10117 Berlin, Germany

[§]Division of Computational Biology, College of Life Sciences, and Division of Physics, School of Engineering, Physics and Mathematics, University of Dundee, Dow Street, Dundee DD1 5EH, U.K.

[∥]Department of Theoretical and Computational Biophysics, Max-Planck-Institute for Biophysical Chemistry, D-37077 Göttingen, Germany

[⊥]Centre of Biophysics and Bioinformatics, Humboldt-Universität zu Berlin, Invalidenstrasse 42, D-10115 Berlin, Germany

S *Supporting Information*

ABSTRACT: G protein coupled receptors (GPCRs) transmit extracellular signals into the cell by binding and activating different intracellular signaling proteins, such as G proteins ($G\alpha\beta\gamma$, families Gi, Gs, Gq, $G_{12/13}$) or arrestins. To address the issue of Gs vs Gi coupling specificity, we carried out molecular dynamics simulations of lipid-embedded active β_2-adrenoceptor (β_2AR^*) in complex with C-terminal peptides derived from the key interaction site of $G\alpha$ ($G\alpha CT$) as surrogate of $G\alpha\beta\gamma$. We find that $Gi\alpha CT$ and $Gs\alpha CT$ exploit distinct cytoplasmic receptor conformations that coexist in the uncomplexed β_2AR^*. The slim $Gi\alpha CT$ stabilizes a β_2AR^* conformation, not accessible to the bulkier $Gs\alpha CT$, which requires a larger TM6 outward tilt for binding. Our results suggest that the TM6 conformational heterogeneity regulates the catalytic activity of β_2AR^* toward Gi or Gs.

G protein coupled receptors (GPCRs) transduce a large variety of extracellular signals into the cell. One and the same receptor can activate different intracellular downstream signaling proteins such as heterotrimeric G proteins ($G\alpha\beta\gamma$, families Gi, Gs, Gq, $G_{12/13}$) or arrestins (arrestin 1–4), resulting in different cellular and physiological responses.[1] Understanding the molecular mechanism of this coupling promiscuity is therefore one of the key questions in current receptor research. The phenomenon that ligands can bias toward arrestin- or G protein-specific signaling, respectively, has been linked to the existence of different conformations of the active receptor (R*), with different G protein and arrestin binding properties.[2] The first structural evidence for how different ligands bias the human β_2-adrenoceptor (β_2AR) toward arrestin or G protein signaling has recently been provided.[3] However, little is known about the structural mechanism by which receptors select between different G protein signaling pathways.[4]

In this study we performed classical all-atom molecular dynamics (MD) simulations to investigate how the conformational space of the active human β_2AR^* is exploited for selective coupling to Gs or Gi. For comparison we chose bovine rhodopsin (RhR), which is capable of interaction with only a single G protein, namely Gt, a member of the Gi family. Our report will focus on the conformational heterogeneity of transmembrane helix 6 (TM6), which is released from the 7-TM helix bundle upon activation, resulting in the prominent outward tilt[5] observed in crystal structures of active GPCRs.[6−9] This hallmark event of GPCR activation leads to the formation of a highly flexible cytoplasmic crevice[10−12] to which the C-terminus of the $G\alpha$ subunit ($G\alpha CT$),[6,7,13,14] a key determinant of G protein coupling specificity,[15] binds. Our present analysis suggests that distinct TM6 outward tilts are responsible for Gi- and Gs-specific signaling by β_2AR^*.

So far, the only crystal structure of a R*·G complex reported is that of β_2AR^* bound to Gs.[7] Comparison with crystal structures of active rhodopsin (RhR*) in complex with $Gt\alpha CT$[6,16,17] reveals that both $G\alpha$ C-termini adopt an α-helical conformation terminated by a reverse turn. $Gs\alpha CT$ and $Gt\alpha CT$ bind with the tip of the reverse turn to $R^{3.50}$ (Ballesteros−Weinstein nomenclature) from the E(D)RY motif at the base of the cytoplasmic crevice of R*. However, the reverse turn of $Gs\alpha CT$ is bulkier than those of $Gt\alpha CT$ and its close homologue $Gi\alpha CT$ (Figure S9). Specifically, the cation−π interaction between Y391 and $R131^{3.50}$ in the β_2AR^*·Gs complex seems to require a 5−6 Å larger TM6 outward tilt than the hydrogen bond between the carbonyl oxygen of C347 and the guanidinium group of $R135^{3.50}$ in RhR*·$Gt\alpha CT$[6] (Figure 1A,B). The present study was thus motivated by the idea that the different space requirements for the key interactions of $Gt\alpha CT$ and $Gs\alpha CT$ with R* result in distinct TM6 outward tilts and differently shaped cytoplasmic crevices in the corresponding complexes (Figure 1C,D).

To find out whether a RhR*-like conformation exists in β_2AR^*, which might be stabilized by $Gi\alpha CT$ and thus be responsible for selective signaling through Gi, a series of MD simulations of the uncomplexed β_2AR^* was started using the receptor coordinates from the β_2AR^*·Gs complex.[7] After *in*
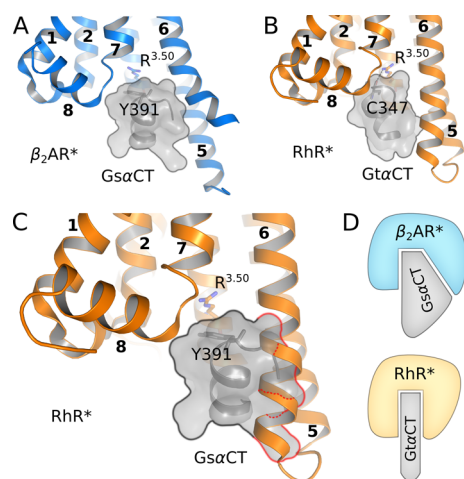
Figure 1. Cytoplasmic crevice of β_2AR* (blue) and RhR* (orange) from complexes with Gs[7] and GtαCT[6] (both in gray ribbon surface representation), respectively. (A−C) Side view: The outward-tilted TM6 of β_2AR* allocates space for the bulky GsαCT (outlined, transparent surface) that would clash (indicated by the red outline in C) with the more inward-tilted TM6 position of RhR* (orange) in complex with GtαCT. R[3.50] from the base of the cytoplasmic crevice and Y391/C347 from the tip of Gs/tαCT are shown as sticks. (D) Schematic representations of the two crystal structure interactions in panels A−C.
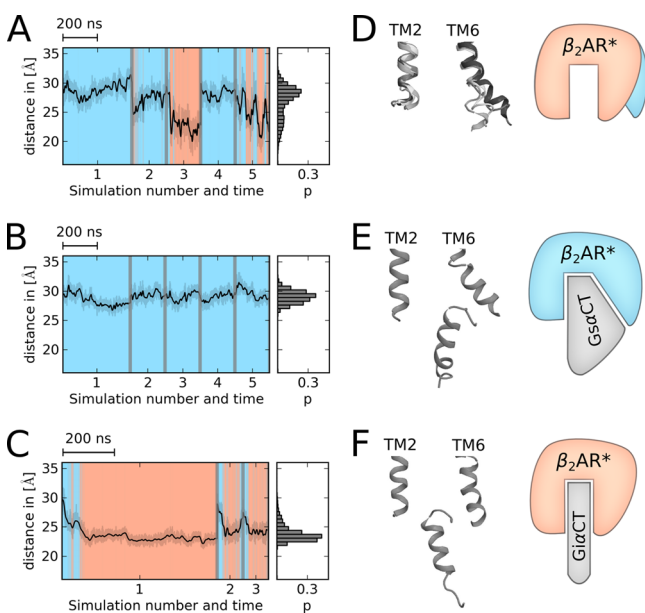
Figure 2. Conformations of the cytoplasmic crevice of β_2AR* observed in MD simulations (A,D) alone, (B,E) with GsαCT$_{19}$, and (C,F) with GiαCT$_{19}$. Panels A−C show the time traces of the TM6 tilts (d_{TM2-6}) with resulting distributions and observed probabilities p. Panels D−F schematically depict the Gs coupled state (blue) and the RhR*-like state of β_2AR* (red) defined by representative TM2 and TM6 conformations. (C) In 3 of 21 simulations (100−600 ns), β_2AR* adopts a RhR*-like conformation with GiαCT$_{19}$. Crystal structures of R and R* exhibit the following TM6 tilts: inactive β_2AR (PDB entry 2RH1), 18.2 Å; β_2AR*·Gs (3SN6), 29.7 Å; inactive RhR (1U19), 16.4 Å; and RhR*·GtαCT (3PQR), 23.2 Å.

silico reconstitution of β_2AR* into a lipid bilayer, five independent 200−400 ns MD simulations were carried out. In accordance with earlier analyses,[10−12] we observe a broad distribution of TM6 tilts in the absence of cytoplasmic binding
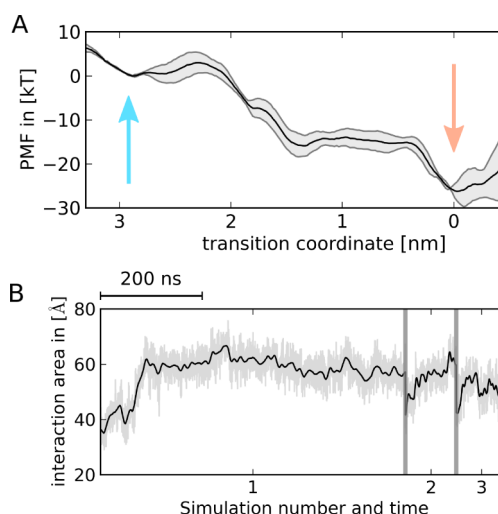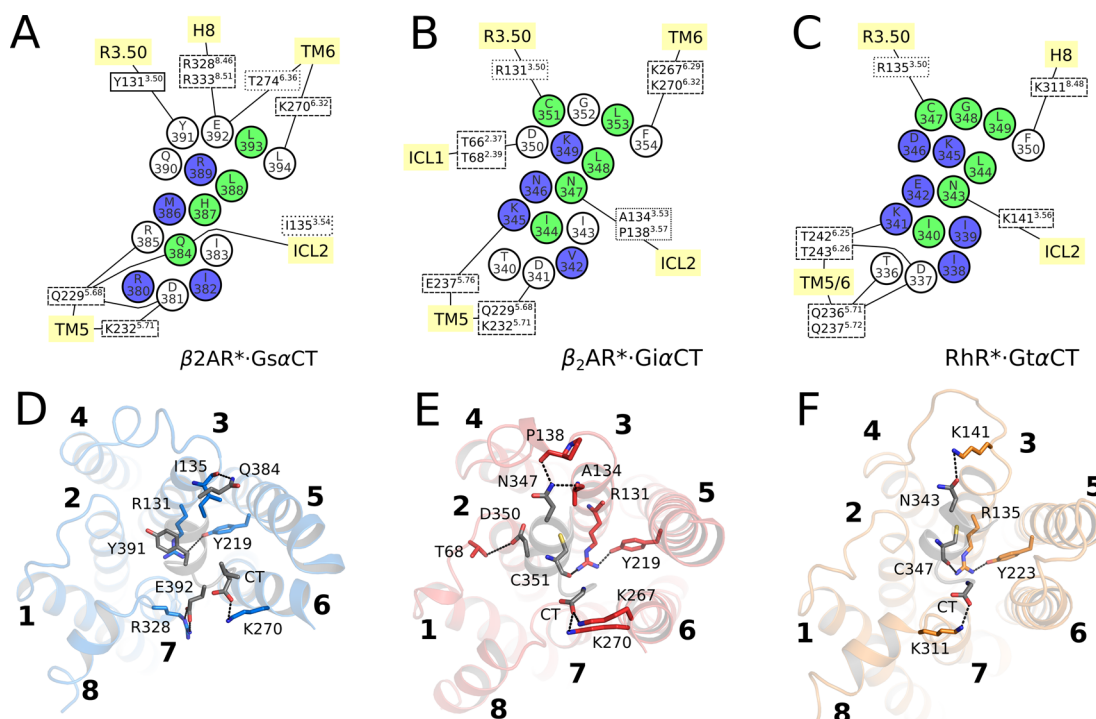

Figure 3. Umbrella sampling run along the coordinates of the TM6 inward movement during transition from the starting state using the receptor coordinates from the β_2AR*·Gs complex to the β_2AR*·GiαCT$_{19}$ complex (see Figure 2C). (A) PMF energy profile (black line) and error estimation (gray area). Arrows indicate the positions of the initial (Gs coupling state, blue) and the final β_2AR* conformation (red) on the transition coordinate (see Supporting Information). An energy barrier of 3.0 ± 2.3 kT is at 2.3 nm on the transition coordinate, which corresponds to $d_{TM2-6} \approx 28.6$ Å. (B) Increase of the β_2AR* GiαCT$_{19}$ interaction surface accompanying the TM6 inward movement.

partners (Figure 2A,D). A pronounced maximum at $d_{TM2-6} = 28$ Å (for definition see SI Methods) reflects that the Gs coupled state is also present in the uncomplexed β_2AR*. A second peak arises around 23 Å, characterizing another population of β_2AR* corresponding to the more closed RhR*·GtαCT state (Figure S1A). Remarkably, during the simulations, TM6 was able to move back and forth between these two states, accompanied by pronounced order-to-disorder transitions of its cytoplasmic end (Figure S1B). This dynamic character is typical for the uncomplexed R*, as has been shown by NMR and FTIR spectroscopy.[11,19] It is noteworthy that for RhR*, which does not couple to Gs,[18] larger TM6 outward tilts corresponding to the β_2AR*·Gs conformation are not observed in MD simulations of uncomplexed RhR* (see ref 11 and Figure S2F).

Selective stabilization of a specific R* conformation out of an ensemble of substates has been suggested as a common mechanism for GPCR-mediated signal transduction.[12,19] In accordance, the β_2AR*·Gs complex reconstituted *in silico* into a lipid bilayer remains essentially unchanged during five 200 ns simulations, although stabilizing mutations, nanobodies, and the fused T4-lysozyme have been eliminated. TM6 (Figure S2A) and GsαCT (Figure S3C) are locked in their positions, and the cation−π interaction between Y391 and R131[3.50] of the receptor persists (Figure S4A). In addition, several other polar and hydrophobic interactions, most of them also present in the crystal structure,[7] fixate GsαCT to ICL2 and ICL3 (Figure S5A).

Gs/iαCT peptides have been used as surrogates of G to examine G protein-selective β_2AR* conformations.[15,20] To identify the minimum peptide length required for complex stabilization, we truncated Gs to a GsαCT 19-mer (GsαCT$_{19}$, [376]FNDCRDIIQRMHLRQYELL[394]). GsαCT$_{19}$ (Figure S3) and TM6 (Figures 2B) remain in their conformations during

11245

dx.doi.org/10.1021/ja5055109 | *J. Am. Chem. Soc.* 2014, 136, 11244−11247

Figure 4. Contacts observed in MD simulations of various R*·GαCT$_{19}$ complexes. (A−C) Recurring polar contacts involving side chains (dashed boxes), backbone carbonyl (dotted boxes), or cation−π interactions (solid boxes) between peptides (circles) and receptors (boxes) depicted as interaction schemes. Buried residues are colored green; accessible residues are blue (see also Figure S8). (D−E) Top view from the intracellular side on the different R*·GαCT$_{19}$ complexes. Hydrogen bonds between residues (sticks) of peptides (gray) and R* (colored) are indicated as dotted lines. For clarity, only the C-terminal 11 residues of the GαCT$_{19}$ peptides are shown in panels D−F, but the full set of interactions is described in panels A−C.

all simulations, stabilized by the same specific interactions as with Gs (Figures S4B and S5B). Further N-terminal truncation to GsαCT$_{11}$ reduces the number of specific contacts with β$_2$AR* (Figures S4C and S5C), leading to a higher positional variability of GsαCT$_{11}$ (Figure S3) and TM6 (Figure S2). Our simulations suggest that the binding interface for Gs coupling to β$_2$AR* consists of 15 C-terminal residues (see Figures 4A, S4A−C, and S5A−C) which form a scaffold between ICL2 and TM5/6, stabilizing the more open cytoplasmic crevice of the Gs coupled receptor. Notably, in simulations of a putative RhR*·GsαCT peptide complex (see SI Methods), the characteristic cation−π interaction between Y391 and R131$^{3.50}$ does not form as with β$_2$AR*·GsαCT (Figure S4), in accordance with the absence of a Gs signaling pathway in the visual RhR system.[21]

Subsequently, we addressed the question whether a Giα C-terminal 19-mer (GiαCT$_{19}$, ^{336}FDAVTDVIIKNNLKD-CGLF^{354}) can stabilize the RhR*-like conformation observed for the uncomplexed β$_2$AR*. The starting position of GiαCT$_{19}$ was extrapolated from the crystal structure complex of GtαCT$_{19}$ (^{332}FDAVTDIIIKENLKDCGLF^{350}) with RhR*.[6] The receptor coordinates were taken from the β$_2$AR*·Gs crystal structure complex.[7] In this starting configuration GiαCT$_{19}$ does not have any contact with TM6. Similar to the simulations of uncomplexed β$_2$AR*, TM6 tends to persist in its starting position within the first hundreds of nanoseconds (Figure S2E). However, in 3 out of 21 independent simulations, the initial receptor conformation is left, and TM6 tilts inward spontaneously by 6 Å (Figure 2C).

To obtain information about the energy barrier that retards formation of the more closed β$_2$AR* state bound to GiαCT

($d_{TM2−6}$ = 23 Å), we performed umbrella sampling (US) MD simulations along one of these trajectories and calculated the potential of mean force (PMF, Figure 3A). The PMFs show that such an energy barrier exists, arising from the reorganization of interactions between TM5/6 (Figure S6B). As soon as this barrier is overcome, the TM6 inward movement follows a continuous downhill reaction. The interaction surface with GiαCT$_{19}$ that remains at its starting position increases (Figure 3B), and the key interaction between C351 and R131$^{3.50}$ forms. This key interaction and a hydrogen bond between N347 and P138$^{3.57}$ from the second intracellular loop (ICL2) and from D341 and K345 to ICL3 are also observed in MD simulations of GtαCT with RhR* (Figures 4C and S5E), supporting the notion that β$_2$AR* forms a complex with GiαCT$_{19}$ very similar to the complex RhR* forms with GtαCT (Figure S7C).

The α-helical content of TM6 increases upon complex formation (Figure S6A), in accordance with our recently proposed model of receptor G protein coupling through structural stabilization of the binding crevice.[11] Extrapolation of the GiαCT$_{19}$ peptide to the Gi holoprotein in a putative β$_2$AR*·Giαβγ complex (model based on β$_2$AR*·Gs[7]) results in a feasible arrangement without clashes (Figure S7A). Finally, our analysis of Gi vs Gs interactions explains previous mutational data, in which a chimeric Gsα/Gtα was capable of binding to and being potently activated by RhR*.[22] The two Gsα triple mutants that made Gsα light-activatable were indeed exchanged at those amino acid positions, where we observe differential interactions of Gs and Gi, namely Y391 to R$^{3.50}$, E392 to TM6/H8 for Gs (Figure 4A) or N347 with ICL2, C351 with R$^{3.50}$, and D350 with ICL1 for Gi (Figure 4B).

11246

dx.doi.org/10.1021/ja5055109 | J. Am. Chem. Soc. 2014, 136, 11244−11247

In accordance with earlier studies,[3,12,19] we observe a strong structural heterogeneity for the two active GPCRs, β_2AR* and RhR*, reflected by broad distributions of different TM6 tilts in the absence of intracellular interaction partners. In the case of β_2AR*, this distribution exhibits at least two pronounced maxima at 23 and 28 Å. The maximum at 28 Å represents the Gs coupled state,[7] while the maximum at 23 Å indicates a second β_2AR* conformation very similar to the one observed in the GtαCT·RhR* complex.[6] GiαCT, a close homologue of GtαCT, stabilizes that more closed β_2AR* conformation while—due to its bulkiness—GsαCT requires the more open cytoplasmic crevice with a much larger TM6 outward tilt for binding. These observations suggest that Gs and Gi/t have different binding modes, both imprinting their own shape onto the cytoplasmic R* crevice through specific interactions of GαCT with β_2AR*.

Our results extend an emerging concept of GPCR signaling based on multiple receptor conformations in equilibrium,[12] each exhibiting specific affinities to the variety of extracellular ligands and intracellular proteins.[2,23,24] In the example studied here, the Gα C-termini of Gs or Gi, representing the key sites for interactions with the active β_2AR*, are able to select and stabilize specific active conformations from a pre-existing equilibrium of agonist-bound receptor states (Figure 2). Thus, the receptor provides a characteristic amount of TM6 flexibility, while the Gα C-terminus selects a specific conformation for productive interaction and signal transfer by presenting a surprisingly small number of crucial residues (Figure 4 and ref 22). Taken together, the abundance of a specific R* conformation, in addition to the availability and affinity of different G proteins, co-determines which pathway prevails in the intracellular network.

ASSOCIATED CONTENT

Ⓢ Supporting Information

Preparation and execution of MD simulations and US calculations, performed and analyzed with GROMACS; GPCRs were selected on the basis of the availability of an X-ray structure of a receptor G protein (or peptides derived thereof) complex, which is a prerequisite for sufficiently accurate atomistic simulations. This material is available free of charge via the Internet at http://pubs.acs.org.

AUTHOR INFORMATION

Corresponding Author

peter.hildebrand@charite.de

Present Address

$^\nabla$M.E.: Jules Stein Eye Institute and Department of Chemistry and Biochemistry, University of California, Los Angeles

Notes

The authors declare no competing financial interest.

REFERENCES

(1) Pierce, K. L.; Premont, R. T.; Lefkowitz, R. J. *Nat. Rev. Mol. Cell. Biol.* **2002**, *3*, 639.

(2) Wisler, J. W.; Xiao, K.; Thomsen, A. R. B.; Lefkowitz, R. J. *Curr. Opin. Cell Biol.* **2014**, *27*, 18.

(3) Liu, J. J.; Horst, R.; Katritch, V.; Stevens, R. C.; Wüthrich, K. *Science* **2012**, *335*, 1106.

(4) Xiao, R. P. *Sci. STKE* **2001**, *2001*, re15.

(5) Altenbach, C.; Kusnetzow, A. K.; Ernst, O. P.; Hofmann, K. P.; Hubbell, W. L. *Proc. Natl. Acad. Sci. U.S.A.* **2008**, *105*, 7439.

(6) Scheerer, P.; Park, J. H.; Hildebrand, P. W.; Kim, Y. J.; Krauss, N.; Choe, H. W.; Hofmann, K. P.; Ernst, O. P. *Nature* **2008**, *455*, 497.

(7) Rasmussen, S. G. F.; DeVree, B. T.; Zou, Y.; Kruse, A. C.; Chung, K. Y.; Kobilka, T. S.; Thian, F. S.; Chae, P. S.; Pardon, E.; Calinski, D.; Mathiesen, J. M.; Shah, S. T. A.; Lyons, J. A.; Caffrey, M.; Gellman, S. H.; Steyaert, J.; Skiniotis, G.; Weis, W. I.; Sunahara, R. K.; Kobilka, B. K. *Nature* **2011**, *477*, 549.

(8) Kruse, A. C.; Ring, A. M.; Manglik, A.; Hu, J.; Hu, K.; Eitel, K.; Hübner, H.; Pardon, E.; Valant, C.; Sexton, P. M.; Christopoulos, A.; Felder, C. C.; Gmeiner, P.; Steyaert, J.; Weis, W. I.; Garcia, K. C.; Wess, J.; Kobilka, B. K. *Nature* **2013**, *504*, 101.

(9) Xu, F.; Wu, H.; Katritch, V.; Han, G. W.; Jacobson, K. a; Gao, Z.-G.; Cherezov, V.; Stevens, R. C. *Science* **2011**, *332*, 322.

(10) Dror, R. O.; Arlow, D. H.; Maragakis, P.; Mildorf, T. J.; Pan, A. C.; Xu, H.; Borhani, D. W.; Shaw, D. E. *Proc. Natl. Acad. Sci. U.S.A.* **2011**, *108*, 18684.

(11) Elgeti, M.; Rose, A. S.; Bartl, F. J.; Hildebrand, P. W.; Hofmann, K. P.; Heck, M. *J. Am. Chem. Soc.* **2013**, *135*, 12305.

(12) Nygaard, R.; Zou, Y.; Dror, R. O.; Mildorf, T. J.; Arlow, D. H.; Manglik, A.; Pan, A. C.; Liu, C. W.; Fung, J. J.; Bokoch, M. P.; Thian, F. S.; Kobilka, T. S.; Shaw, D. E.; Mueller, L.; Prosser, R. S.; Kobilka, B. K. *Cell* **2013**, *152*, 532.

(13) Hamm, H. E.; Deretic, D.; Arendt, A.; Hargrave, P. A.; Koenig, B.; Hofmann, K. P. *Science* **1988**, *241*, 832.

(14) Kisselev, O. G.; Kao, J.; Ponder, J. W.; Fann, Y. C.; Gautam, N.; Marshall, G. R. *Proc. Natl. Acad. Sci. U.S.A.* **1998**, *95*, 4270.

(15) Oldham, W. M.; Hamm, H. E. *Nat. Rev. Mol. Cell. Biol.* **2008**, *9*, 60.

(16) Choe, H.-W.; Kim, Y. J.; Park, J. H.; Morizumi, T.; Pai, E. F.; Krauss, N.; Hofmann, K. P.; Scheerer, P.; Ernst, O. P. *Nature* **2011**, *471*, 651.

(17) Standfuss, J.; Edwards, P. C.; D'Antona, A.; Fransen, M.; Xie, G.; Oprian, D. D.; Schertler, G. F. X. *Nature* **2011**, *471*, 656.

(18) Cerione, R. A.; Staniszewski, C.; Benovic, J. L.; Lefkowitz, R. J.; Caron, M. G.; Gierschik, P.; Somers, R.; Spiegel, A. M.; Codina, J.; Birnbaumer, L. *J. Biol. Chem.* **1985**, *260*, 1493.

(19) Kim, T. H.; Chung, K. Y.; Manglik, A.; Hansen, A. L.; Dror, R. O.; Mildorf, T. J.; Shaw, D. E.; Kobilka, B. K.; Prosser, R. S. *J. Am. Chem. Soc.* **2013**, *135*, 9465.

(20) Malik, R. U.; Ritt, M.; DeVree, B. T.; Neubig, R. R.; Sunahara, R. K.; Sivaramakrishnan, S. *J. Biol. Chem.* **2013**, *288*, 17167.

(21) Hepler, J. R.; Gilman, A. G. *Trends Biochem. Sci.* **1992**, *17*, 383.

(22) Natochin, M.; Muradov, K. G.; McEntaffer, R. L.; Artemyev, N. O. *J. Biol. Chem.* **2000**, *275*, 2669.

(23) Rahmeh, R.; Damian, M.; Cottet, M.; Orcel, H.; Mendre, C.; Durroux, T.; Sharma, K. S.; Durand, G.; Pucci, B.; Trinquet, E.; Zwier, J. M.; Deupi, X.; Bron, P.; Banères, J.-L.; Mouillac, B.; Granier, S. *Proc. Natl. Acad. Sci. U.S.A.* **2012**, *109*, 6733.

(24) Soriano-Úrsúa, M. A.; Trujillo-Ferrara, J. G.; Correa-Basurto, J.; Vilar, S. *J. Med. Chem.* **2013**, *56*, 8207.